Article

Cell

Asprosin, a Fasting-Induced Glucogenic Protein Hormone

Graphical Abstract

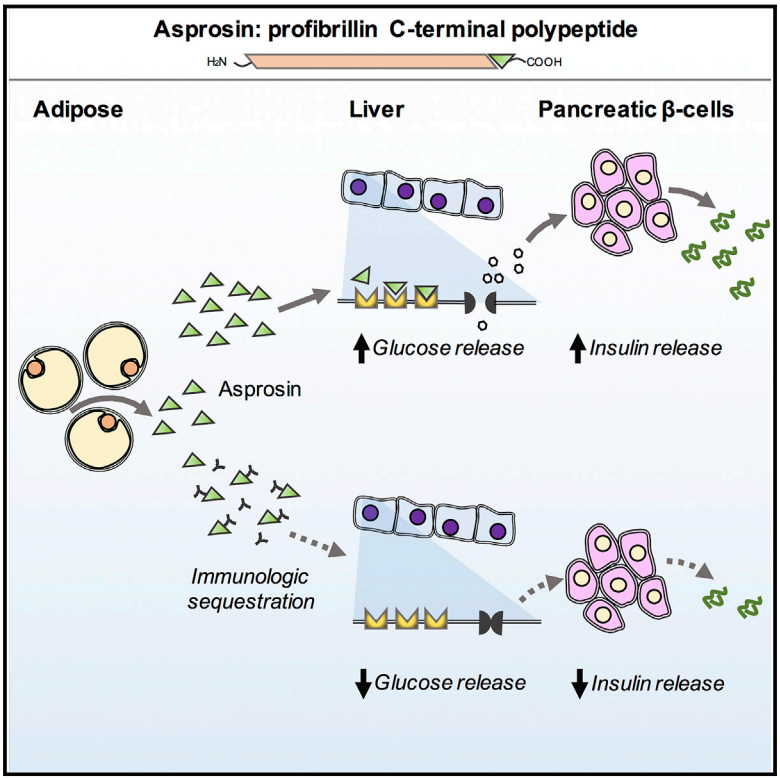

Highlights

- Asprosin discovered as a fasting-induced glucogenic protein hormone
- Asprosin induces hepatic glucose production by using cAMP as a second messenger
- Asprosin is pathologically elevated with human and mouse insulin resistance
- Reduction of asprosin protects against metabolic-syndrome-associated hyperinsulinism

Authors

Chase Romere, Clemens Duerrschmid, Juan Bournat, ..., Nancy F. Butte, David D. Moore, Atul R. Chopra

Correspondence

chopra@bcm.edu

In Brief

Circulating asprosin, a protein hormone, responds to low dietary glucose by triggering the release of liver glucose stores, and the reduction of asprosin protects against the hyperinsulinism associated with metabolic syndrome.

Romere et al., 2016, Cell *165*, 1–14
April 21, 2016
http://dx.doi.org/10.1016/j.cell.2016.02.063

CellPress

Please cite this article in press as: Romere et al., Asprosin, a Fasting-Induced Glucogenic Protein Hormone, Cell (2016), http://dx.doi.org/10.1016/j.cell.2016.02.063

Article

Cell

Asprosin, a Fasting-Induced Glucogenic Protein Hormone

Chase Romere,[1] Clemens Duerrschmid,[1] Juan Bournat,[1] Petra Constable,[1] Mahim Jain,[2] Fan Xia,[2] Pradip K. Saha,[1] Maria Del Solar,[6] Bokai Zhu,[1] Brian York,[1] Poonam Sarkar,[3] David A. Rendon,[3] M. Waleed Gaber,[3] Scott A. LeMaire,[4] Joseph S. Coselli,[4] Dianna M. Milewicz,[5] V. Reid Sutton,[2] Nancy F. Butte,[3] David D. Moore,[1] and Atul R. Chopra[1,2,*]

[1]Department of Molecular and Cellular Biology, Baylor College of Medicine, Houston, TX 77030, USA
[2]Department of Molecular and Human Genetics, Baylor College of Medicine, Houston, TX 77030, USA
[3]Department of Pediatrics, Baylor College of Medicine, Houston, TX 77030, USA
[4]Division of Cardiothoracic Surgery, Michael E. DeBakey Department of Surgery, Baylor College of Medicine, Houston, TX 77030, USA
[5]Department of Internal Medicine, University of Texas Medical School at Houston, Houston, TX 77030, USA
[6]Department of Pharmacology and Systems Therapeutics, Icahn School of Medicine at Mount Sinai, New York, NY 10029, USA
*Correspondence: chopra@bcm.edu
http://dx.doi.org/10.1016/j.cell.2016.02.063

SUMMARY

Hepatic glucose release into the circulation is vital for brain function and survival during periods of fasting and is modulated by an array of hormones that precisely regulate plasma glucose levels. We have identified a fasting-induced protein hormone that modulates hepatic glucose release. It is the C-terminal cleavage product of profibrillin, and we name it Asprosin. Asprosin is secreted by white adipose, circulates at nanomolar levels, and is recruited to the liver, where it activates the G protein-cAMP-PKA pathway, resulting in rapid glucose release into the circulation. Humans and mice with insulin resistance show pathologically elevated plasma asprosin, and its loss of function via immunologic or genetic means has a profound glucose- and insulin-lowering effect secondary to reduced hepatic glucose release. Asprosin represents a glucogenic protein hormone, and therapeutically targeting it may be beneficial in type II diabetes and metabolic syndrome.

INTRODUCTION

Hormones, their receptors, and the associated signaling pathways make compelling drug targets because of their wide-ranging biological significance (Behrens and Bromer, 1958). Protein hormones, as a subclass, have defining characteristics. They usually (but not always) result from cleavage of a larger pro-protein and, upon secretion, traffic via the circulation to a target organ. There they bind a target cell using a cell-surface receptor, displaying high affinity, saturability, and ability to be competed off. They stimulate rapid signal transduction using a second-messenger system, followed by a measurable physiological consequence. Given the brain's strict dependence on glucose as a fuel, plasma glucose levels are precisely regulated by an array of hormones (Aronoff et al., 2004). Some are secreted in response to nutritional cues, while others respond to glucose itself, producing highly coordinated and precise regulation of circulating glucose levels. Perturbations in this system can cause pathological alteration in glucose levels, often with severe consequences.

We have discovered a protein hormone that regulates glucose homeostasis. It is the C-terminal cleavage product of profibrillin (encoded by *FBN1*). Its absence in humans results in a unique pattern of metabolic dysregulation that includes partial lipodystrophy, accompanied by reduced plasma insulin, while maintaining euglycemia. We name it Asprosin, after the Greek word for white ($\alpha\sigma\pi\rho o\sigma$), because of the reduction in subcutaneous white adipose tissue that is displayed by asprosin-deficient patients and because white adipose tissue appears to be a source of plasma asprosin.

RESULTS

Neonatal Progeroid Syndrome Mutations Reduce Plasma Insulin Levels while Maintaining Euglycemia in Humans

Neonatal progeroid syndrome (NPS) was first described in 1977 (OMIM: 264090) and is characterized by congenital, partial lipodystrophy, predominantly affecting the face and extremities (O'Neill et al., 2007). Although NPS patients appear progeroid because of facial dysmorphic features and reduced subcutaneous fat, the term is a misnomer as the patients do not display accelerated aging. We identified two unrelated individuals with NPS. We examined their glucose and insulin homeostasis status, since both partial and generalized lipodystrophic disorders are frequently associated with insulin resistance (Bindlish et al., 2015). Contrary to this notion, overnight-fasted plasma insulin levels from our NPS patients were 2-fold lower than unaffected subjects, while maintaining euglycemia (Figure 1A).

Whole-exome and Sanger sequencing identified de novo, heterozygous 3′ truncating mutations in *FBN1* in both patients (Figures 1B and 1C). Upon reaching the genetic diagnosis, we searched the literature for similar cases and discovered five single-patient case reports of NPS associated with *FBN1* 3′ truncating mutations (Goldblatt et al., 2011; Graul-Neumann et al., 2010; Horn and Robinson, 2011; Jacquinet et al., 2014; Takenouchi et al., 2013). All seven subjects, including the two reported herein, were diagnosed with NPS, and all have truncating

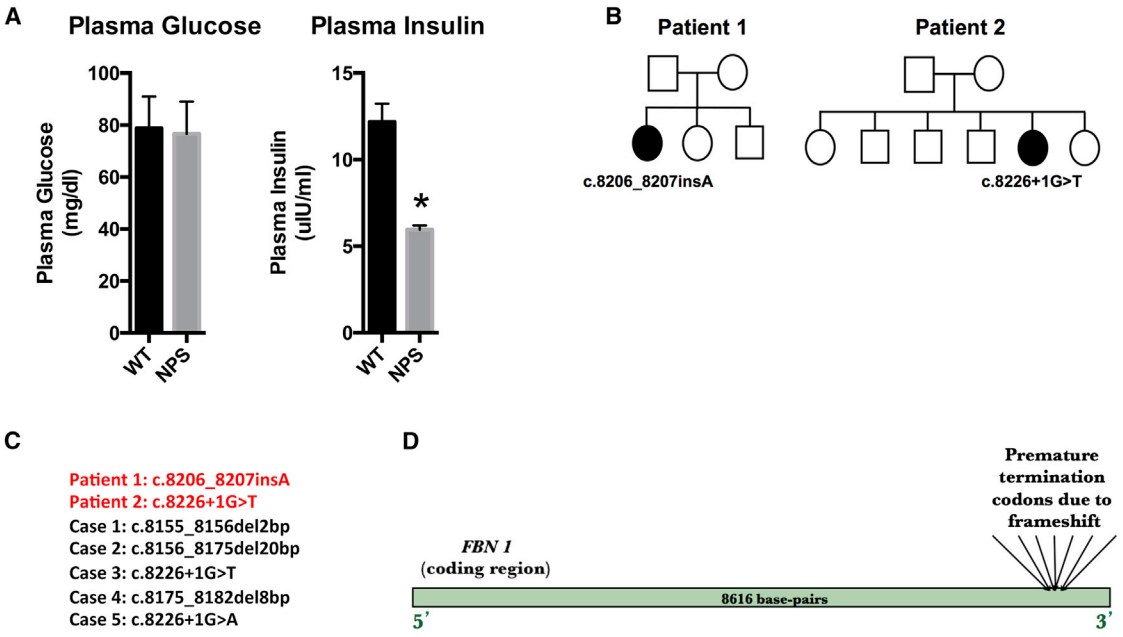

E

WT

2641 QFSGGCQDINECGSAQAPCSYGCSNTEGGYLCGCPPGYFRIGQGHCVSGMGMGRGNPEPP
2701 VSGEMDDNSLSPEACYECKINGYPKRGRKRRSTNETDASNIEDQSETEANVSLASWDVEK
2761 TAIFAFNISHVSNKVRILELLPALTTLTNHNRYLIESGNEDGFFKINQKEGISYLHFTKK
2821 KPVAGTYSLQISSTPLYKKKELNQLEDKYDKDYLSGELGDNLKMKIQVLLH*

Patient #1

2641 QFSGGCQDINECGSAQAPCSYGCSNTEGGYLCGCPPGYFRIGQGHCVSGMGMGRGNPEPP
2701 VSGEMDDNSLSPEACYECKINGYPKRGRKRRSTNENN*

Patient #2

2641 QFSGGCQDINECGSAQAPCSYGCSNTEGGYLCGCPPGYFRIGQISLRQKPM*

Case 1

2641 QFSGGCQDINECGSAQAPCSYGCSNTEGGYLCGCPPGYFRIGQGHCVSGMGMGRGNPEPP
2701 VSGEMDDNSLSPEACYECDQWLPQTGQETEKHKRN*

Case 2

2641 QFSGGCQDINECGSAQAPCSYGCSNTEGGYLCGCPPGYFRIGQGHCVSGMGMGRGNPEPP
2701 VSGEMDDNSLSPEACYECTGQETEKHKRN*

Case 3

2641 QFSGGCQDINECGSAQAPCSYGCSNTEGGYLCGCPPGYFRIGQISLRQKPM*

Case 4

2641 QFSGGCQDINECGSAQAPCSYGCSNTEGGYLCGCPPGYFRIGQGHCVSGMGMGRGNPEPP
2701 VSGEMDDNSLSPEACYECKINGYPKETEKHKRN*

Case 5

2641 QFSGGCQDINECGSAQAPCSYGCSNTEGGYLCGCPPGYFRIGQISLRQKPM*

Figure 1. NPS Mutations Reduce Plasma Insulin Levels while Maintaining Euglycemia in Humans

(A) Overnight fasted plasma glucose and insulin levels from two NPS patients (NPS) and four unaffected control subjects (WT).
(B) *FBN1* mutations and family pedigrees of the two NPS patients in (A). Standard pedigree symbols are used with affected status noted by filled symbols.
(C) 3′ *FBN1* mutations in seven NPS patients; two reported herein and five from published case reports. Patient #2 also has a heterozygous missense variant (c.8222T > C) in *FBN1* that is predicted to be benign and is not indicated in the figure for clarity.
(D) Schematic depicting the clustering of the NPS mutations at the 3′ end of the *FBN1* gene.

(legend continued on next page)

mutations within a 71-bp segment at the 3′ end of the *FBN1* coding region, displaying tight genotype-phenotype correlation (Figure 1D). All seven mutations occur 3′ to the last 50 nt of the penultimate exon and are therefore predicted to escape mRNA nonsense-mediated decay (NMD), leading to expression of a mutant, truncated profibrillin protein (Figure 1E).

Profibrillin is translated as a 2,871-amino-acid long proprotein, which is cleaved at the C terminus by the protease furin (Lönnqvist et al., 1998; Milewicz et al., 1995). This generates a 140-amino-acid long C-terminal cleavage product, in addition to mature fibrillin-1 (an extracellular matrix component). All seven NPS mutations are clustered around the cleavage site, resulting in heterozygous ablation of the C-terminal cleavage product (asprosin) (Figure 1E), whose fate and function were unknown.

Asprosin, the C-Terminal Cleavage Product of Profibrillin, Is a Fasting-Responsive Plasma Protein

Asprosin is encoded by the ultimate two exons of *FBN1*. Exon 65 encodes 11 amino acids, while exon 66 encodes 129 amino acids. Together, those two exons display a somewhat higher vertebrate evolutionary conservation score compared with the rest of the profibrillin coding sequence (Figures S1A and S1B). We developed an asprosin-specific monoclonal antibody and validated its specificity for asprosin using *Fbn1* wild-type (WT) and null cells (Figure S1C). Immunoblotting human plasma with the anti-asprosin antibody shows a single protein running on SDS-PAGE at ~30 kDa, while bacterially expressed recombinant asprosin runs at ~17 kDa (Figure 2A). Asprosin is predicted to have three N-linked glycosylation sites and potentially other post-translational modifications that are lacking in bacteria (Figures S1D and S1E). This likely explains the difference in molecular weight between mammalian and bacterially expressed asprosin. Indeed, using mammalian cells for expression of asprosin produced a protein that was secreted into the media and ran on SDS-PAGE at the same molecular weight (~30 kDa) (Lönnqvist et al., 1998) as we observed in human plasma, cell lysates and media from mouse embryonic fibroblasts, and cell/tissue lysates from cultured adipocytes and mouse white adipose tissue (Figures 2A, S1C, S2A, and S2B).

To measure circulating asprosin levels, we developed a sandwich ELISA (Figure S3A). We constructed a standard curve using recombinant asprosin and used it to calculate plasma and media levels (Figure 2B). As expected, the asprosin sandwich ELISA displayed high specificity using media from WT and *Fbn1*−/− cells (Figure S3C). Asprosin was found to be present in plasma at consistent nanomolar levels in humans, mice, and rats (Figure 2C). Interestingly, NPS patients displayed a greater reduction in circulating asprosin level than predicted from their heterozygous genotype, compared not only with WT control subjects but also when compared with patients that have heterozygous truncations of profibrillin sufficiently N-terminal so as to undergo mRNA nonsense-mediated decay (Figure 2D). This suggests that the mutant profibrillin that is predicted to be expressed in NPS cells (due to escape from mRNA NMD) exerts a dominant-negative effect on secretion of asprosin from the WT allele. We tested this concept by overexpressing the truncated, mutant version of profibrillin in WT cells and found that this interfered with the ability of those cells to secrete asprosin into the media, compared with overexpression of an irrelevant protein, such as GFP (Figures S3E and S3F).

To assess daily fluctuations in circulating asprosin concentrations, mice were kept in a 12-hr light/12-hr dark cycle for 7 days to establish entrainment and were subsequently kept in constant darkness. Plasma was then isolated from these mice at 4-hr intervals and subjected to asprosin ELISA analysis. We found that plasma asprosin displays circadian oscillation with an acute drop in levels coinciding with the onset of feeding (Figure 2E). In the opposite direction, overnight fasting in humans, mice, and rats resulted in increased circulating asprosin (Figure 2F).

Adipose Tissue Generates and Secretes Asprosin

We examined the *FBN1* mRNA profile across all human tissues using the Genotype-Tissue Expression Project (GTex) RNaseq dataset and found that adipose tissue demonstrated the highest *FBN1* mRNA expression across all tissues (Figure 2G). To confirm this in mice, we assessed the *Fbn1* expression profile across various metabolically important organs. Consistent with the human profile, we found that white adipose tissue displayed the highest *Fbn1* mRNA expression (Figure 2H). Given that white adipose tissue is a well-known endocrine organ (Trayhurn et al., 2006), we examined whether it could serve as a source of circulating asprosin. We assessed plasma levels of asprosin in mice that had been subjected to genetic ablation of adipose tissue. We used *Bscl2*−/− mice for this purpose. *BSCL2* deficiency results in Berardinelli-Seip congenital lipodystrophy in humans (knockout mice mimic this phenotype) with a 60%–70% reduction in adipose tissue (Cui et al., 2011). In such mice we detected a ~2-fold reduction in plasma asprosin (Figure 2I). The next experimental strategy we employed was to assess whether adipocytes in culture were capable of generating and secreting asprosin. For this, we differentiated two distinct adipogenic cell lines, 3T3-L1 and a mesenchymal stem cell line (C3H10T1/2), into mature adipocytes (Figures 2J and 2K) and subjected the cell culture media to asprosin protein analysis. We found robust accumulation of asprosin in serum-free culture media from mature adipocytes, but not from preadipocytes (Figures 2J and 2K), suggesting that adipocytes are capable of generating and secreting asprosin.

A Single Dose of Recombinant Asprosin Elevates Blood Glucose and Insulin in Mice

We employed ectopic overexpression of full-length *FBN1* using an adenovirus in the hope that the transduced organ (in this case, the liver, which normally shows low endogenous *FBN1* expression [Figures 2G and 2H] and is the primary target of adenoviral infection) would process the resultant profibrillin

(E) All seven NPS mutations are clustered around the furin cleavage site (RGRKRR motif highlighted in yellow) and are predicted to result in heterozygous ablation of the 140-amino-acid C-terminal polypeptide (asprosin). Non-native amino acids due to a frameshift are shown in red. Patient #2, case 3, and case 5 have a mutation in a splice-donor site that has been predicted to produce the indicated mutant protein (Jacquinet et al., 2014).
Data are represented as the mean ± SEM.

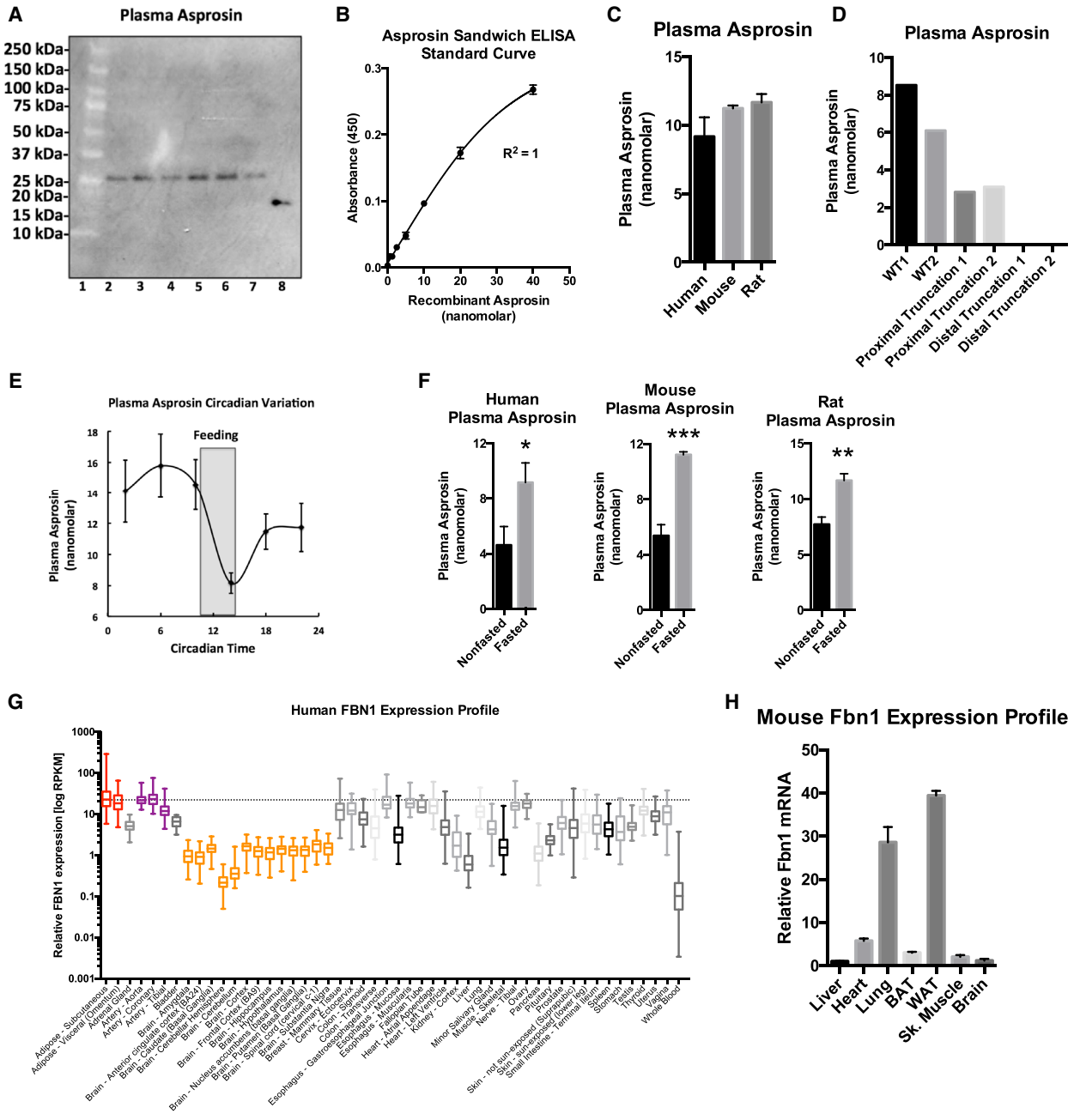

(legend on next page)

and secrete asprosin into the circulation. This strategy showed robust overexpression of profibrillin protein in the liver and a 2-fold elevation in plasma asprosin (Figures 3A and 3B). The second strategy involved daily subcutaneous injection of bacterially expressed asprosin (validated to result in a 50 nM peak level 20 min after injection; Figure 5D) or recombinant GFP as a control. 10 days of exposure to increased plasma asprosin in either a continuous (adenoviral overexpression) or pulsatile fashion (daily recombinant asprosin injection) resulted in elevated glucose and insulin levels in 2-hr fasted mice using both experimental strategies (Figures 3C and 3D). This result demonstrated that bacterially expressed recombinant asprosin retains the biological activity displayed by its endogenously expressed counterpart and that elevation of circulating asprosin is sufficient to increase blood glucose and insulin levels.

In order to understand acute responses, we injected a single dose of recombinant asprosin subcutaneously in mice that had been subjected to a preceding 2-hr fast, and measured plasma glucose at 15, 30, 60, and 120 min post-injection. Mice were denied access to food through the length of the experiment. A single asprosin dose resulted in an immediate spike in blood glucose levels (Figure 3E). This resulted in compensatory hyperinsulinemia (measured at the 15-min time point) (Figure 3F), which normalized blood glucose levels by 60 min post-injection (Figure 3E). Similar results were obtained in mice that were subjected to a preceding overnight fast, although the rate of the resultant blood glucose spike was somewhat slower, likely due to fasting-induced depletion of glucogenic substrates (Figures 3G and 3H). These results implicated the liver as the target organ for asprosin due to its role as the primary site for stored glucose (as glycogen), which is rapidly released into the circulation during fasting. Interestingly, asprosin treatment had no effect on plasma levels of catabolic hormones (glucagon, catecholamines, and glucocorticoids), known to induce hepatic glucose release (Figure 3I).

Asprosin Targets the Liver to Increase Plasma Glucose in a Cell-Autonomous Manner

Glucose and insulin tolerance tests in mice exposed to a single dose of recombinant asprosin showed little evidence of altered glucose uptake (in response to insulin) in peripheral organs, such as muscle or fat (unchanged slope of glucose disposal), but showed altered peak glucose levels, again implicating the liver (Figures 4A and 4B). To confirm the liver as the site of asprosin action, we performed the hyperinsulinemic-euglycemic clamp. This test unequivocally showed that elevated plasma asprosin results in increased hepatic glucose production (Figure 4C), but has no impact on the ability of peripheral organs to take up glucose in response to insulin (Figure 4D). To test whether the effect of asprosin on the liver is cell autonomous, we exposed isolated primary mouse hepatocytes to increasing concentrations of recombinant asprosin or GFP for 2 hr. Media from cells exposed to asprosin showed an increase in glucose concentration in a dose-dependent manner, demonstrating a direct effect of asprosin on hepatocytes (Figure 4E).

Asprosin Traffics to the Liver In Vivo and Binds the Hepatocyte Surface with High Affinity in a Saturable and Competitive Manner

We labeled recombinant asprosin with iodine-125 (I^{125}) and injected it intravenously in mice, followed by single-photon emission computerized tomography (SPECT) scans to identify sites of accumulation. An equivalent amount of free I^{125} or I^{125}-Asprosin that was boiled for 5 min (to induce loss of the asprosin tertiary structure) was used as a control. In contrast to the accumulation patterns for free I^{125} and boiled I^{125}-Asprosin, SPECT scans in coronal and axial planes (Figure 5A), and mean liver photon intensity (Figure 5B), both showed that I^{125}-Asprosin trafficked primarily to the liver and that asprosin's tertiary structure was essential for its liver recruitment. In accord with liver trafficking, gamma counting of blood and viscera showed that recombinant blood asprosin levels decrease in concert with the increased liver levels (Figure 5C). To measure plasma half-life, we used a sandwich ELISA system targeting the N-terminal His-tag on the recombinant asprosin protein at 15, 30, 60, and 120 min following subcutaneous injection. Consistent with our results using IV infusion of I^{125}-Asprosin, plasma His-tagged asprosin showed a half-life of approximately 20 min and a peak level of 50 nM that was achieved 20 min post-injection (Figure 5D).

To examine specific binding of asprosin by hepatocytes, we incubated mouse primary hepatocytes with an increasing

Figure 2. Asprosin, the C-Terminal Cleavage Product of Profibrillin, Is a Fasting-Responsive Plasma Protein

(A) Asprosin immunoblot on six individual human plasma samples (lanes 2–7). Bacterially expressed recombinant asprosin was used as a positive control (lane 8). The molecular weight marker is shown in lane 1.

(B) Asprosin sandwich ELISA standard curve.

(C) Sandwich ELISA was used to measure plasma asprosin levels in overnight fasted humans, mice, and rats (n = 7 in each group).

(D) Sandwich ELISA was used to measure plasma asprosin levels in unaffected control subjects (WT), two patients with heterozygous *FBN1* frameshift mutations 5′ to the threshold for mRNA nonsense-mediated decay (c.6769-6773del5, c.1328-23_c.1339del35insTTATTTTATT) (proximal truncation 1&2), and two NPS patients (distal truncation 1&2).

(E) Sandwich ELISA was used to measure plasma asprosin every 4 hr from circadian C57Bl/6 mice entrained to total darkness (n = 5). The period of feeding is shaded.

(F) Sandwich ELISA was used to measure plasma asprosin levels in ad libitum fed or overnight fasted humans, mice, and rats (n = 7 in each group).

(G) *FBN1* expression across all human tissues using the GTEx human RNaseq database.

(H) Various WT C57Bl/6 mouse organs were assessed for *Fbn1* mRNA expression by qPCR.

(I) Plasma asprosin was assessed using sandwich ELISA on plasma from 13-week-old, 6-hr fasted male WT and *Bscl2*-null mice.

(J) *PPARγ2* mRNA expression by qPCR and media asprosin by sandwich ELISA were assessed on cultured 3T3-L1 cells with or without exposure to an adipogenic cocktail for 7 days. Cells were washed with PBS and then exposed to glucose-free, serum-free media for 24 hr for assessment of secretion.

(K) C3H10T1/2 cells were subjected to the same analysis as in (J).

Data are represented as the mean ± SEM. See also Figures S1, S2, and S3.

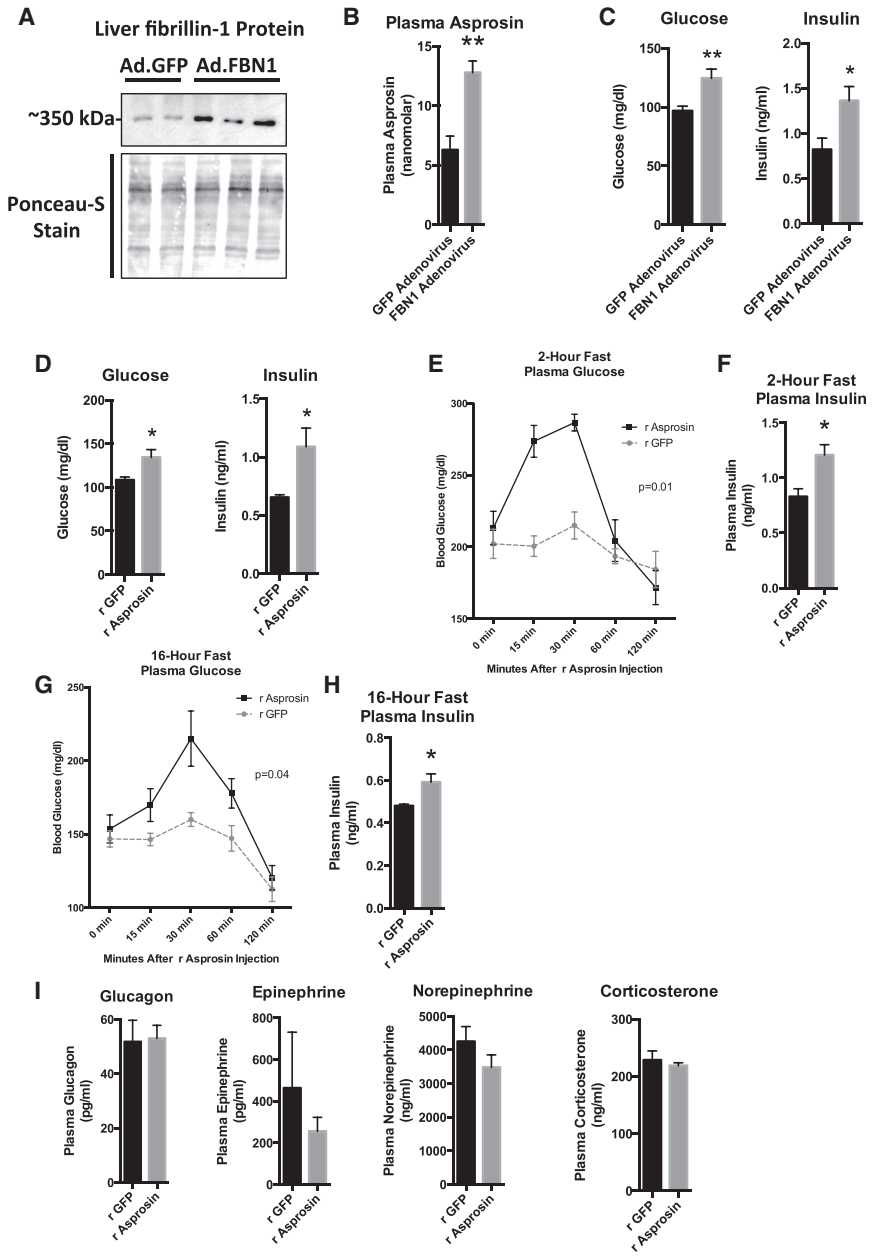

Figure 3. Increase in Circulating Asprosin Is Associated with Elevated Blood Glucose and Insulin in Mice

(A) Profibrillin (350 kDa) immunoblot on liver lysates 10 days after WT mice were subjected to a one-time tail vein injection of 10^{11} viral particles of adenovirus carrying cDNA for *FBN1* (lanes 3, 4, and 5) or *GFP* (lanes 1 and 2). Mice were subjected to a 2-hr fast for synchronization prior to sacrifice.

(B) Sandwich ELISA was used to measure plasma asprosin levels from mice in (A) (n = 5 in each group).

(C) Plasma glucose and insulin levels from mice in (A) (n = 5 in each group).

(D) Plasma glucose and insulin levels were measured 10 days after WT mice were subjected to daily subcutaneous injection of 30 μg recombinant asprosin (validated to result in a 50 nM peak plasma level) or recombinant GFP for 10 days (n = 5 in each group).

(E) Plasma glucose was measured at the indicated times after a single 30 μg dose of subcutaneous recombinant asprosin or GFP in mice that had been subjected to a 2-hr fast prior to injection (n = 6 in each group). Two-way ANOVA with Bonferroni post test was used to calculate the p value.

(F) Plasma insulin was measured 15 min after injection from mice in (E) (n = 6 in each group).

(G) Plasma glucose was measured at the indicated times after a single 30 μg dose of subcutaneous recombinant asprosin or GFP in mice that had been subjected to an overnight (~16 hr) fast prior to injection (n = 6 in each group). Two-way ANOVA with Bonferroni post test was used to calculate the p value.

(H) Plasma insulin was measured 30 min after injection from mice in (G) (n = 6 in each group).

(I) Plasma glucagon, catecholamines, and corticosterone were measured 15–20 min after a single 30 μg dose of subcutaneous recombinant asprosin or GFP in mice that had been subjected to a 2-hr fast prior to injection (n = 6 in each group).

Data are represented as the mean ± SEM.

amount of an asprosin-biotin conjugate, washed with PBS, and measured the relative level of biotin at the hepatocyte surface. Asprosin bound the hepatocyte surface in a dose-responsive and saturable manner (Figure 5E). Repeating the same procedure in the presence of 100-fold excess unconjugated asprosin abolished the effect, suggesting competition for potential receptor binding sites (Figure 5E).

Asprosin Uses the cAMP Second-Messenger System and Activates Protein Kinase A in the Liver

Exposing mice to a single 30-μg dose of recombinant asprosin for 20 min (validated to result in a 50-nM peak level) was sufficient to increase liver cyclic AMP (cAMP) and protein kinase A (PKA) activity (Figures 6A–6C). Identical results were obtained upon incubating mouse primary hepatocytes with recombinant asprosin for 10 min (Figures 6D and 6E). Hepatocyte PKA activity increased in a dose-responsive manner upon addition of recombinant asprosin (Figure 6F), similar to what we observed with hepatocyte glucose release (Figure 4E). The effects of asprosin on both hepatocyte glucose release and PKA activation were blocked by suramin, a general heterotrimeric G protein inhibitor (Figures 6G and 6H). In addition, asprosin-mediated hepatocyte glucose release could be blocked by using cAMPS-Rp, a competitive antagonist of cAMP binding to PKA (Figure 6I). These results demonstrate that asprosin increases hepatocyte glucose release by employing the G protein-cAMP-PKA axis in vivo and in vitro. Because glucagon and catecholamines also employ the same intracellular signaling axis, we tested the impact of inhibiting the glucagon

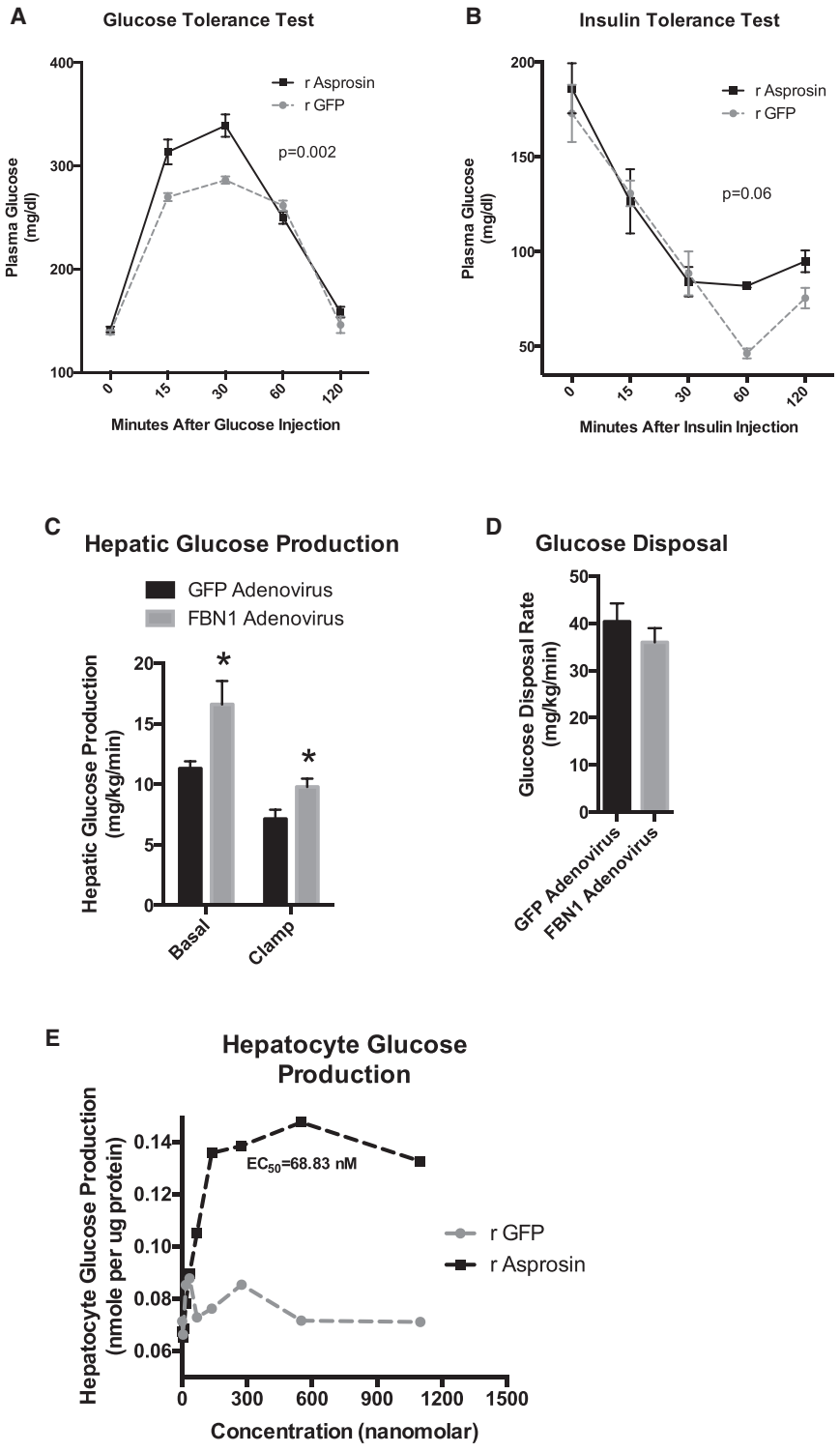

Figure 4. In a Cell-Autonomous Effect, Asprosin Targets the Liver to Increase Plasma Glucose

(A) A glucose tolerance test was performed 2 hr following a subcutaneous injection with 30 μg recombinant asprosin or GFP in WT mice fasted for 2 hr for synchronization prior to injection (n = 6 mice in each group). Two-way ANOVA with Bonferroni post test was used to calculate the p value.

(B) An insulin tolerance test was performed 2 hr following subcutaneous injection with 30 μg recombinant asprosin or GFP in WT mice fasted for 2 hr for synchronization prior to injection (n = 6 mice in each group). Two-way ANOVA with Bonferroni post test was used to calculate the p value.

(C) Basal (18 hr fasted) and clamped hepatic glucose production was measured using the hyperinsulinemic-euglycemic clamp 10 days after WT mice were subjected to a one-time tail vein injection of 10^{11} viral particles of adenovirus carrying cDNA for *FBN1* or *GFP* (n = 7 mice in each group).

(D) Glucose disposal rate was measured in mice from (C) (n = 7 mice in each group).

(E) Media glucose accumulation was measured 2 hr after incubating mouse primary hepatocytes with 0, 4, 8, 16, 32, 64, 138, 275, 550, or 1,100 nM recombinant asprosin or GFP, 1 hr following isolation of cells from WT mice, without plating the cells.

Data are represented as the mean ± SEM.

receptor or the β-adrenergic receptor on the ability of asprosin to enhance hepatocyte glucose release. While the respective inhibitors completely blocked the effects of glucagon or epinephrine, they had no impact on the ability of asprosin to influence hepatocyte glucose release (Figures 6J and 6K). This suggests that asprosin uses a cell-surface receptor system that is distinct from those used by glucagon and catecholamines. Since insulin is known to induce a reduction in intracellular cAMP (via activation of the G_{ai} pathway), we tested whether insulin would oppose asprosin's effect on hepatocyte PKA activation and glucose release, which is demonstrated to be due to an increase in intracellular cAMP. Indeed, we found that insulin suppressed asprosin-mediated hepatocyte PKA activation (Figure 6L) and glucose release (Figure 6M).

Asprosin Immunologic Sequestration Is Protective against Metabolic-Syndrome-Associated Hyperinsulinism

We found that plasma asprosin levels are pathologically elevated in human subjects with insulin resistance (Figure 7A). Similar elevations were seen in two independent mouse models of insulin resistance (diet-induced obesity and *Ob* mutation) (Figure 7B). Intraperitoneal injection of a single dose of an asprosin-specific monoclonal antibody was sufficient to acutely drop plasma asprosin levels at 3 and 6 hr post-injection, with recovery to normal levels at 24 hr (Figure 7C). Both

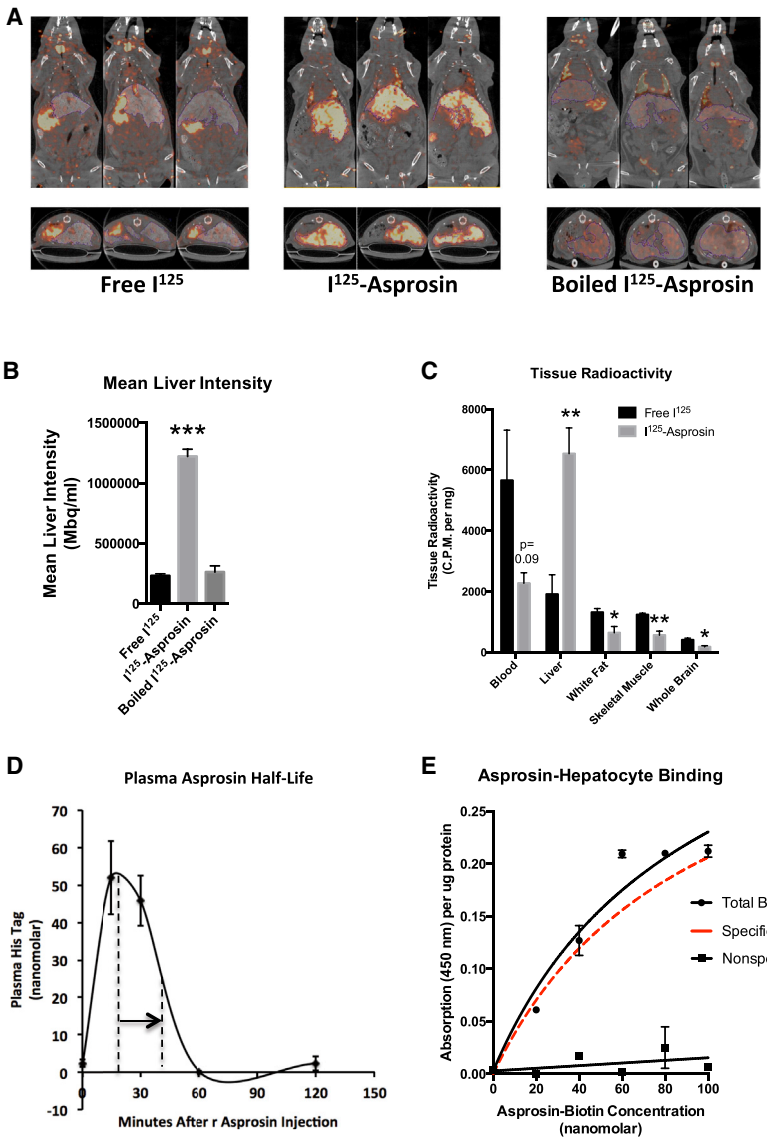

Figure 5. Asprosin Traffics to the Liver In Vivo and Binds the Hepatocyte Surface with High Affinity in a Saturable and Competitive Manner

(A) SPECT scans were performed 15 min after intravenous injection with 150 μCi I^{125}-asprosin, boiled I^{125}-asprosin, or free I^{125} in live, anesthetized mice previously injected with bismuth as a hepatic contrast agent. Three representative images are shown in axial and coronal planes.

(B) Liver asprosin accumulation was measured as liver photon intensity from mice in (A).

(C) Tissue radioactivity (normalized to tissue weight) was measured using a γ-counter after sacrificing mice from (A), 45 min following injection (n = 4 mice).

(D) Sandwich ELISA was used to measure plasma His tag (recombinant asprosin contains an N-terminal His tag) in WT mice before injection and 15, 30, 60, and 120 min after injection with 30 μg recombinant asprosin. The time taken for peak signal to fall to half-maximal level is indicated by the arrow.

(E) The level of biotin at the hepatocyte surface was measured using a colorimetric assay upon incubation of unplated mouse primary hepatocytes with increasing concentration of a recombinant asprosin-biotin conjugate, with (non-specific binding) or without (total binding) 100-fold excess recombinant asprosin in the media. Specific binding (shown in red) was calculated as the difference between the two curves.

Data are represented as the mean ± SEM.

ad-libitum-fed (following a 2-hr fast for synchronization) models of mouse insulin resistance showed an acute reduction in plasma insulin levels (while maintaining euglycemia), concurrent with plasma asprosin depletion (Figures 7D–7G). To directly test the effect of loss of asprosin on hepatocyte glucose production without the potential insulin compensatory effect, we treated mouse primary hepatocytes with the asprosin-specific antibody prior to incubating them with asprosin. As expected, the asprosin-specific antibody blocked asprosin-mediated hepatocyte glucose release, while a non-specific control antibody had no effect (Figure S3D).

To validate immunologic sequestration as a legitimate loss-of-function strategy, we tested *FBN1* hypomorphic mice (homozygous MgR mice), which express only ~20% of the WT *FBN1* transcript (Pereira et al., 1999). MgR mice displayed a 70% decrease in circulating asprosin (Figure 7H). Upon 2 hr of fasting, MgR mice displayed a 2-fold deficit in plasma insulin, while maintaining euglycemia (similar to what we observed with immunologic sequestration of asprosin in ad-libitum-fed mice) (Figures 7I and 7J). However, upon 24 hr of fasting, a physiologic situation that eliminates insulin from the circulation of mice (Figure 7J), MgR mice displayed fasting hypoglycemia (Figure 7I), suggesting that insulin's buffering effect needs to be eliminated (via a long fast) to unmask the reduction in plasma glucose induced by asprosin loss of function. To confirm this, we performed a hyperinsulinemic-euglycemic clamp study on MgR mice that had been fasted for ~18 hr (basal). Under such conditions, we found an acute deficit in hepatic glucose production (HGP) in MgR mice compared with WT mice (Figure 7K). This result is consistent with clamp results showing an increase in HGP upon asprosin gain of function (Figures 4C and 4D). Expectedly, neither clamp study demonstrated a change in whole-body glucose disposal (insulin sensitivity) (Figures 4D and 7L), suggesting that asprosin's effect on glucose homeostasis is limited to serving as a stimulator of HGP (Figure S4), and any change in plasma insulin levels is indirect and downstream of the change in HGP.

Finally, a single subcutaneous administration of asprosin in overnight-fasted MgR mice was sufficient to completely rescue the insulin deficiency displayed by these mice (Figure 7M). This result demonstrates that the insulin deficiency displayed by MgR mice is entirely due to a deficiency in circulating asprosin,

and not to some indirect effect of their decreased expression of functional fibrillin protein.

DISCUSSION

Whether circulating asprosin concentration is experimentally decreased (genetic depletion in NPS patients, genetic depletion in MgR mice, or acute removal via immunologic sequestration in mice) or increased (adenovirus-mediated overexpression or direct recombinant protein injection), the result is a corresponding change in plasma glucose and insulin. With asprosin loss of function, hypoglycemia is only unmasked upon elimination of a β-cell-mediated corrective action, by fasting mice long enough to drive insulin levels close to zero, leaving little room for β cells to further decrease insulin secretion and normalize plasma glucose.

It seems surprising that a nutritionally responsive hormone that displays circadian oscillation (Figure 2E) would be derived from what would seem a relatively "static" structural/ECM protein. This led us to examine the profile of the *FBN1* transcript using a publicly available circadiomics database (http://circadiomics.igb.uci.edu). Interestingly, the *Fbn1* transcript displays robust daily circadian oscillation in several tissues, such as the heart, adrenal, lung, white fat, and kidney. The notion that fibrillin-1 is a static, structural molecule may need further examination. Another pertinent question relates to the primary tissue of origin of asprosin. We demonstrate adipose to be one of the sources of plasma asprosin. This observation is consistent with the known function of adipose as an endocrine organ and a sensor/modulator of energy homeostasis. However, it is worth noting that organs besides adipose could also serve as sources of plasma asprosin, given the fairly high expression of *FBN1* in several organs.

Since asprosin functions to increase plasma glucose levels, and circulating asprosin levels are increased by fasting (a baseline glucose condition) (Figure 2F) and decreased by feeding (a high glucose condition) (Figure 2E), we hypothesized that glucose could serve as a suppressor of plasma asprosin levels in a negative-feedback loop. To determine this, we subjected mature adipocytes in culture to high glucose levels and found that this treatment was sufficient to strongly inhibit the accumulation of asprosin in media, compared with adipocytes subjected to glucose-free conditions (Figures S5B and S5D). We detected no decrease in intracellular asprosin protein with glucose addition (Figure S5E), suggesting that glucose-mediated downregulation of extracellular asprosin levels does not occur at the level of transcription, biosynthesis, or processing. To confirm this result in vivo, we subjected WT mice to streptozotocin (STZ) treatment, which is known to ablate pancreatic β cells, resulting in high blood glucose. In such mice plasma asprosin was found to be far lower than in mice with normal blood glucose (Figure S5F). Together, these in vitro and in vivo results are consistent with the notion that glucose serves as a negative influencer of plasma asprosin levels in a negative-feedback loop and is consistent with the regulation of other major hormones (for example, calcium suppresses parathyroid hormone secretion and glucose suppresses glucagon secretion) (Campbell and Drucker, 2015; Dumoulin et al., 1995).

Generally, protein hormones are processed via endoplasmic reticulum and Golgi pathways and stored in intracellular granules, followed by secretion in response to appropriate cues. Consistent with this, we detected processed asprosin intracellularly in cultured fibroblasts, mouse white adipose tissue, and cultured adipocytes (Figures S1C, S2A, and S2B). Asprosin has been shown to retain the ability to be secreted from the cell, despite the lack of a signal peptide. This was demonstrated by overexpressing just the asprosin coding exons in mammalian cells, followed by detection of asprosin in the media (Lönnqvist et al., 1998). We repeated this assay by overexpressing asprosin-encoding cDNA in *Fbn1*−/− cells (to prevent contamination from endogenous asprosin), and asprosin secretion was detected in the media (Figures S6A and S6B). Furthermore, asprosin secretion could be suppressed by glucose (Figure S6B), consistent with the phenomenon observed in cultured adipocytes (Figures S5B and S5D). Several extracellular proteins, such as FGF-1, FGF-2, and IL-1β, lack an N-terminal signal peptide and are secreted using non-classical or leaderless secretion (Nickel, 2003), as demonstrated by asprosin.

To assess the tissue sources of elevated asprosin with insulin resistance, we assessed the *Fbn1* mRNA profile across various mouse tissues from WT and *Ob/Ob* mice. We found strong upregulation of the *Fbn1* mRNA in white adipose tissue, brown adipose tissue, and skeletal muscle (Figure S7A), three organs that are frequently implicated in the pathogenesis of insulin resistance. The upregulation in white adipose tissue was especially potent, again implicating it as a major tissue source of plasma asprosin. The mechanism of upregulation of plasma asprosin via increased *Fbn1* mRNA in adipose and skeletal muscle seems unique to the pathogenesis of insulin resistance because we did not detect any changes in *Fbn1* mRNA in any of the organs with fasting and streptozotocin treatment (Figures S7B and S7C), two other manipulations associated with major changes in plasma asprosin. Type II diabetes remains a major cause of morbidity, in isolation, and as a part of metabolic syndrome. Inappropriately, elevated glucose production by the insulin-resistant liver is a major factor underlying its pathogenesis (Magnusson et al., 1992). It is possible that the elevated asprosin levels we observed in insulin-resistant humans and mice contribute to this. The insulin-lowering effects of immunologic sequestration of asprosin in obese, insulin-resistant mice suggest decreased asprosin activity as a unique approach to acutely counteract this pathologic effect. Accordingly, asprosin depletion may represent an important therapeutic strategy against type II diabetes.

EXPERIMENTAL PROCEDURES

Study Subjects and Ethics Statement

Informed consent and permission to use biological materials for research was obtained prior to participation from all subjects under one of four Institutional Review Board-approved protocols at Baylor College of Medicine.

Clinical Evaluation

Study subjects were assessed by clinical history, physical examination, and family history. After informed consent, plasma isolation, BMI measurements, and body-fat percentage measurements (DEXA) were carried out with standard universal precautions.

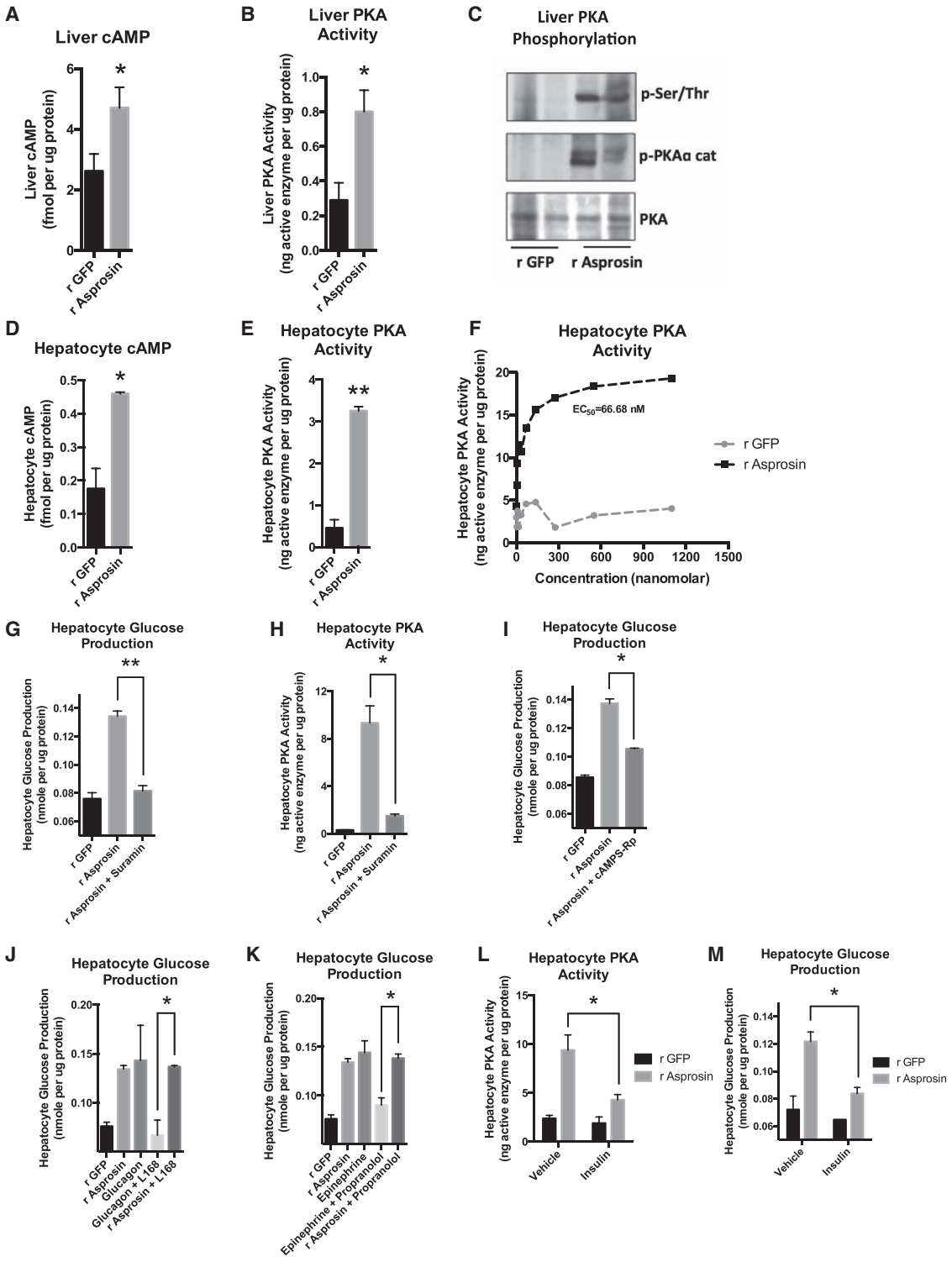

Figure 6. Asprosin Uses the cAMP Second-Messenger System and Activates PKA in the Liver

(A) Liver cAMP level was measured 15 min after a single 30-μg dose of subcutaneous recombinant asprosin or GFP in mice that had been subjected to a 2-hr fast prior to injection (n = 6 in each group).

(B) Liver PKA activity was measured in mice from (A).

(C) Immunoblot analysis for phosphorylated PKA catalytic subunit or for phosphorylated serine/threonine PKA substrate was performed on liver lysates from mice in (A).

(legend continued on next page)

Whole-Exome Capture and Sequencing

Genomic DNA from patient #1 and her parents was subjected to whole-exome sequencing (trio analysis). Variants were annotated, and analysis was performed in the trio to look for potential recessive (homozygous and compound heterozygous) and de novo variants.

Sanger Sequencing

Genomic DNA from both patients was subjected to Sanger sequencing. Primers were designed to encompass exons 65 and 66, including intron-exon boundaries, of the *FBN1* gene using Primer3. Sanger reads were analyzed using the Lasergene Seqman software. For patient #1, Sanger sequencing was performed on genomic DNA from both parents and unaffected siblings to confirm de novo occurrence and segregation with the phenotype.

Animals

We used 12-week-old male WT C57Bl/6 mice for in vivo studies. MgR heterozygous mice were obtained from Jackson labs and bred to obtain male MgR homozygous mice and WT littermates. 5-week-old male Ob/Ob mice were obtained from Jackson labs. Mice were housed 2–5 per cage in a 12-hr light/12-hr dark cycle with ad libitum access to food and water. For diet-induced obesity studies, mice were placed on the adjusted-calories diet providing 60% of calories from fat by Harlan-Teklad for 12 weeks. Mice were exposed to adenoviral-mediated transgenesis (10^{11} virus particles per mouse) via tail-vein injections. Mice were exposed to 30 μg recombinant His-tagged asprosin or recombinant GFP daily for 10 days via subcutaneous injection. Mice were sacrificed, and plasma and various organs were isolated 10 days after virus or peptide injection. For single-dose injections, the same protocol was followed as that for daily injections, followed by collection of plasma at the indicated times via tail bleeds for insulin and glucose measurement. Insulin and glucose tolerance tests (ITT and GTT) were performed using standard procedures. A 0.5 U/kg insulin bolus was used for the ITT, and a 1.5 mg/g glucose bolus was used for the GTT. For immunologic sequestration experiments, mice were injected intraperitoneally with a 500-μg dose in saline of a custom-built (Thermo Scientific) anti-asprosin mouse monoclonal antibody directed against amino acids 106–134 (human profibrillin amino acids 2838–2865) or an equivalent dose of isotype-matched immunoglobulin G (IgG) (Southern Biotech). Hyperinsulinemic-euglycemic clamp studies were performed in unrestrained mice using regular human insulin (Humulin R, doses: 2.5 mU/kg body weight) in combination with high-performance liquid chromatography-purified [3-3H] glucose as described previously (Saha et al., 2010). The Baylor College of Medicine Institutional Animal Care and Utilization Committee approved all experiments.

Plasma Metabolic Parameters

Human plasma insulin was measured using a human insulin ELISA kit by Abcam. Mouse plasma insulin was measured using a mouse insulin ELISA kit by Millipore. Mouse plasma glucagon, epinephrine, norepinephrine, and corticosterone were measured by the Vanderbilt University Hormone Assay & Analytical Services Core.

Recombinant Asprosin and GFP

Human *FBN1* (2732–2871 amino acids) cDNA was cloned and subsequently sub-cloned into a pET-22B vector for expression in *Escherichia coli*. The fusion protein that was expressed in *E. coli* is 146 amino acids long comprising of a six-amino-acid His tag on the N terminus and a 140-amino-acid wild-type asprosin. His-tagged GFP expressed in *E. coli* was obtained from Thermo Scientific as the control protein. The His-asprosin and His-GFP were isolated from *E. coli* and allowed to bind to Ni-NTA His-Bind column. After extensive washing of the column in order to remove contaminating proteins, His-asprosin and His-GFP were eluted from the column using a 150-mM imidazole buffer. The recombinant proteins were further purified using size-exclusion columns and polymyxin B-based endotoxin-depletion columns (Detoxi-Gel Endotoxin Removing Gel by Thermo Scientific) with as many passages as required to bring the final endotoxin concentration equal to or below 2 EU/ml, and buffer exchanged into a PBS-glycerol buffer or a 20 mM MOPS (pH 7.0), 300 mM NaCl, and 150 mM Imidazole buffer. The purified proteins were subjected to SDS-PAGE analysis in order to determine the purity level. The His-GFP and His-asprosin proteins used in all recombinant protein experiments were >90% pure with endotoxin levels (determined using the Pierce LAL Chromogenic Endotoxin Quantitation Kit) as indicated (Figure S7D) before and after passage through endotoxin-depletion columns.

Cell Culture

Primary mouse hepatocytes were isolated from 8- to 12-week-old WT mice using standard methodology. Within a few minutes of isolation, cells were placed in glucose-free media in Eppendorf tubes and subjected to treatment with recombinant 50 nM asprosin, 50 nM recombinant GFP, 5 μM Suramin (Tocris), 200 μM cAMPS-Rp (Tocris), 1 μM L168,049 (Tocris), 100 μM Epinephrine (Sigma), 10 μg/ml Glucagon (Sigma), 10 mg/l Insulin (Sigma), or 100 μM Propranolol (Sigma). The cells were treated with 50 nM recombinant asprosin or GFP for 10 min for cAMP and PKA assays and for 2 hr for the in vitro glucose production assay. Cells were pretreated with various inhibitors for 1 hr prior to treatment with asprosin, GFP, glucagon, or epinephrine. cAMP was measured from cell lysates using the cAMP Direct Immunoassay Kit from Cell Biolabs. PKA activity was measured from cell lysates using the PKA Kinase Activity Kit from Enzo Lifesciences. Media glucose content was measured using the Glucose Colorimetric Assay Kit from Biovision. Results were normalized to protein content.

Recombinant asprosin was conjugated with biotin using the Basic Biotinylation Sulfo-NHS Kit from Pierce. Primary hepatocytes were incubated with increasing concentration of the asprosin-biotin conjugate at 4°C, alone, or in the presence of 100-fold excess unconjugated asprosin for 30 min. The cells were washed three times with PBS without lysis, followed by addition

(D) Hepatocyte cAMP level was measured 10 min after incubating mouse primary hepatocytes with 50 nM recombinant asprosin, 1 hr following isolation of cells from WT mice, without plating the cells.
(E) Hepatocyte PKA activity was measured in samples from (D).
(F) Hepatocyte PKA activity was measured upon 2 hr of incubation of mouse primary hepatocytes with 0, 4, 8, 16, 32, 64, 138, 275, 550, or 1,100 nM recombinant asprosin or GFP, 1 hr following isolation of cells from WT mice, without plating the cells.
(G) Media glucose accumulation was measured 2 hr after incubating mouse primary hepatocytes with 50 nM recombinant asprosin or GFP, with or without a G protein inhibitor (Suramin) (5 μM), 1 hr following isolation of cells from WT mice, without plating the cells.
(H) Hepatocyte PKA activity was measured in samples from (G).
(I) Media glucose accumulation was measured 2 hr after incubating mouse primary hepatocytes with 50 nM recombinant asprosin or GFP, with or without a competitive antagonist of cAMP-induced activation of PKA (cAMPS-Rp) (200 μM), 1 hr following isolation of cells from WT mice, without plating the cells.
(J) Media glucose accumulation was measured 2 hr after incubating mouse primary hepatocytes with 50 nM recombinant asprosin or GFP, or 10 μg/ml glucagon, with or without a non-competitive antagonist of the glucagon receptor (L168,049) (1 μM) 1 hr following isolation of cells from WT mice, without plating the cells.
(K) The same analysis was performed as in (J) using 100 μM epinephrine, with or without an antagonist of the β-adrenergic receptor (propranolol) (100 μM). The r GFP and r asprosin controls are common for (J) and (K).
(L) Hepatocyte PKA activity was measured 2 hr after incubating mouse primary hepatocytes with 50 nM recombinant asprosin or GFP, with vehicle or 10 mg/l insulin, 1 hr following isolation of cells from WT mice, without plating the cells.
(M) Hepatocyte glucose production was measured in samples from (L).
Data are represented as the mean ± SEM.

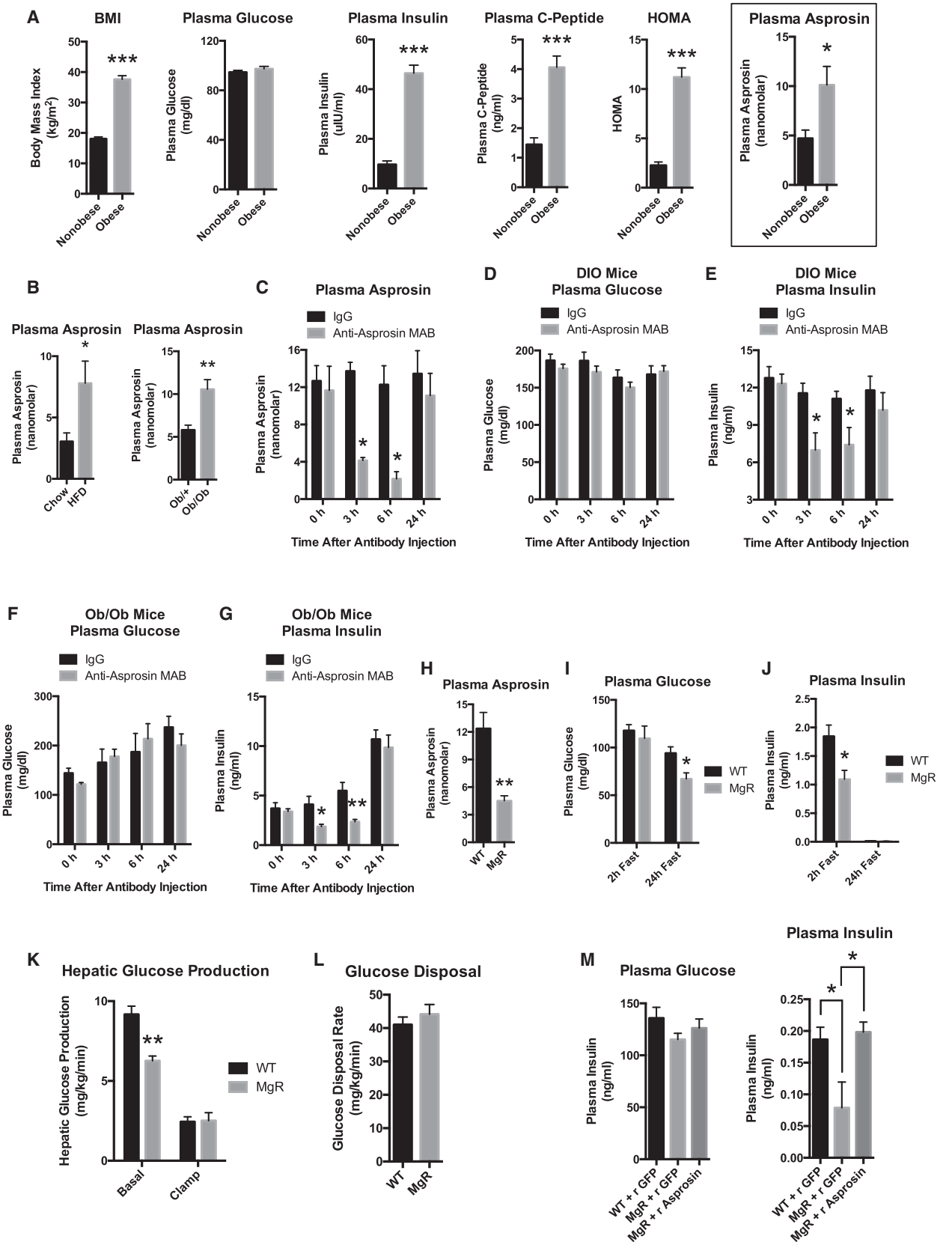

(legend on next page)

of streptavidin-HRP. The resultant absorbance was measured colorimetrically, and the results were normalized to protein content.

3T3-L1 and C3H10T1/2 preadipocyte cells were exposed to an adipogenic cocktail (1 μM insulin, 1 μM dexamethasone, 0.5 mM isobutyl methyl xanthine, and 3 μM rosiglitazone) for 7 days. Adipogenesis was confirmed by visualization of lipid droplets and *PPARg2* mRNA expression.

Serum-free DMEM, with or without 4.5 g/l glucose, was used for measuring glucose-mediated influence on secretion of asprosin.

WT human 140-amino-acid asprosin (profibrillin amino acids 2732–2871) and mutant profibrillin carrying the c.8206_8207InsA mutation that induces a frameshift and C-terminal truncation were sub-cloned under the control of the CMV promoter using the pCMV6-Neo vector system.

Sandwich ELISA and Western Blot

For the endogenous asprosin sandwich ELISA, a custom-built (Thermo Scientific) mouse monoclonal anti-asprosin antibody against asprosin amino acids 106–134 (human profibrillin amino acids 2838–2865) was used as the capture antibody, and a goat anti-asprosin polyclonal antibody against asprosin amino acids 6–19 (human profibrillin amino acids 2737–2750) by Abnova was used as the detection antibody. An anti-goat secondary antibody linked to HRP was used to generate a signal. For the His-tag sandwich ELISA, the same procedure was used, except for the use of a goat anti-His polyclonal antibody (Abcam) as the detection antibody. Increasing amounts of recombinant asprosin (which contains an N-terminal His tag) were used to generate a standard curve for both assays. EDTA plasma was used for plasma sandwich ELISAs, and serum-free DMEM concentrated using Vivaspin protein concentrator spin columns by GE Life Sciences was used for media sandwich ELISAs.

Plasma western blotting for asprosin was done using a custom-built (Thermo Scientific) mouse monoclonal anti-asprosin antibody against asprosin amino acids 106–134 (human profibrillin amino acids 2838–2865). Plasma was depleted of immunoglobulins and albumin using an Albumin/IgG Removal Kit by Pierce.

Western blotting for profibrillin was done using the mouse monoclonal anti-fibrillin-1 antibody against profibrillin amino acids 451–909 by Abcam.

Western blotting for phospho-PKA and total PKA was carried out using antibodies from Santa Cruz Biotechnology.

Statistical Methods

All results are presented as mean ± SEM. p values are calculated by unpaired Student's t test for all results, except where indicated by two-way ANOVA. *$p < 0.05$, **$p < 0.01$, and ***$p < 0.001$.

ACCESSION NUMBERS

The accession number for the whole exome sequencing data pertaining to patient #1 reported in this paper has been uploaded to [SRA]: SRS876533.

SUPPLEMENTAL INFORMATION

Supplemental Information includes Supplemental Experimental Procedures and seven figures and can be found with this article online at http://dx.doi.org/10.1016/j.cell.2016.02.063.

AUTHOR CONTRIBUTIONS

Conceptualization, A.R.C.; Basic Investigation, C.R., C.D., J.B., P.C., M.J., F.X., P.K.S., M.D.S., P.S., D.A.R., and A.R.C.; Clinical Investigation, V.R.S., N.F.B., and A.R.C; Resources, B.Z., B.Y., M.W.G., S.A.L., J.S.C., D.M.M., and D.D.M.; Writing, D.D.M. and A.R.C.

ACKNOWLEDGMENTS

The work was supported by the Baylor-Johns Hopkins Center for Mendelian Genomics, funded by the NHGRI (U54HG006542), supported by the Mouse Metabolic Core at BCM, funded by the NIH (P30 DK079638), supported by the Thoracic Aortic Disease Tissue Bank at BCM, and funded by the NIH (P50 HL083794). The Vanderbilt University Hormone Assay Core is supported by NIH grants (DK059637 and DK020593). The Genotype-Tissue Expression (GTEx) Project is supported by the Common Fund of the Office of the Director of the NIH (additional funds were provided by the NCI, NHGRI, NHLBI, NIDA, NIMH, and NINDS). We thank Texas Children's Hospital for the use of the Small Animal Imaging facility. The laboratory of Francesco Ramirez at the Mt. Sinai School of Medicine originally generated MgR (*Fbn1* hypomorphic) mice. *Fbn1*-null and WT mouse embryonic fibroblasts were a kind gift from Dan Rifkin. Plasma from *Bscl2*-null and WT mice was a kind gift from Xavier Prieur and Weiqin Chen. A.R.C. is supported by the NIDDK (1K08DK102529), the Chao Physician-Scientist Award, the Caroline Weiss Law scholar award, and a departmental laboratory start-up package.

Received: October 7, 2015
Revised: December 29, 2015
Accepted: February 23, 2016
Published: April 14, 2016

Figure 7. Immunologic or Genetic Asprosin Loss of Function Reduces Hepatic Glucose Production, Plasma Glucose, and Plasma Insulin

(A) Sandwich ELISA was used to measure plasma asprosin levels in eight obese, insulin-resistant male human subjects and eight non-obese, sex- and age-matched control subjects. Pertinent physiological parameters are also presented.

(B) Sandwich ELISA was used to measure plasma asprosin levels in male WT mice that had been subjected to a high-fat diet (60% of calories from fat) or normal chow for 12 weeks and from 5-week-old male Ob/+ or Ob/Ob mice upon 2 hr of fasting for synchronization (n = 5 mice in each group).

(C) Sandwich ELISA was used to measure plasma asprosin levels at the indicated times after intraperitoneal injection of 500 μg of IgG or anti-asprosin monoclonal antibody, with ad libitum feeding following a 2-hr fast for synchronization, in male WT mice that had been subjected to a high-fat diet (60% of calories from fat) for 12 weeks (n = 6 mice in each group).

(D) Plasma glucose was measured in mice from (C).

(E) Plasma insulin was measured in mice from (C).

(F) Plasma glucose was measured at the indicated times in 5-week-old male WT or Ob/Ob mice after intraperitoneal injection of 500 μg of IgG or anti-asprosin monoclonal antibody, with ad libitum feeding following a 2-hr fast for synchronization (n = 6 mice in each group).

(G) Plasma insulin was measured in mice from (F).

(H) Sandwich ELISA was used to measure plasma asprosin levels in male WT or homozygous MgR mice following a 2-hr fast for synchronization (n = 5 mice in each group).

(I) Plasma glucose was measured in male WT or homozygous MgR mice following a 2-hr fast or following a 24-hr fast (n = 5–7 mice in each group).

(J) Plasma insulin was measured in mice from (I).

(K) Basal (18-hr fasted) and clamped hepatic glucose production was measured using the hyperinsulinemic-euglycemic clamp in 10-week-old WT or homozygous MgR mice (n = 6 mice in each group).

(L) The glucose disposal rate was measured in mice from (K) (n = 6 mice in each group).

(M) Plasma glucose and insulin were measured in WT or homozygous male MgR mice following an overnight fast, 30 min after subcutaneous injection of 30 μg recombinant asprosin or GFP (n = 5–7 mice in each group).

Data are represented as the mean ± SEM. See also Figures S4, S5, S6, and S7.

REFERENCES

Aronoff, S.L., Berkowitz, K., and Shreiner, B. (2004). Glucose metabolism and regulation: beyond insulin and glucagon. Diabetes Spectr. *17*, 183–190.

Behrens, O.K., and Bromer, W.W. (1958). Biochemistry of the protein hormones. Annu. Rev. Biochem. *27*, 57–100.

Bindlish, S., Presswala, L.S., and Schwartz, F. (2015). Lipodystrophy: syndrome of severe insulin resistance. Postgrad. Med. *127*, 511–516.

Campbell, J.E., and Drucker, D.J. (2015). Islet α cells and glucagon–critical regulators of energy homeostasis. Nat. Rev. Endocrinol. *11*, 329–338.

Cui, X., Wang, Y., Tang, Y., Liu, Y., Zhao, L., Deng, J., Xu, G., Peng, X., Ju, S., Liu, G., and Yang, H. (2011). Seipin ablation in mice results in severe generalized lipodystrophy. Hum. Mol. Genet. *20*, 3022–3030.

Dumoulin, G., Hory, B., Nguyen, N.U., Henriet, M.T., Bresson, C., Regnard, J., and Saint-Hillier, Y. (1995). Acute oral calcium load decreases parathyroid secretion and suppresses tubular phosphate loss in long-term renal transplant recipients. Am. J. Nephrol. *15*, 238–244.

Goldblatt, J., Hyatt, J., Edwards, C., and Walpole, I. (2011). Further evidence for a marfanoid syndrome with neonatal progeroid features and severe generalized lipodystrophy due to frameshift mutations near the 3′ end of the FBN1 gene. Am. J. Med. Genet. A. *155A*, 717–720.

Graul-Neumann, L.M., Kienitz, T., Robinson, P.N., Baasanjav, S., Karow, B., Gillessen-Kaesbach, G., Fahsold, R., Schmidt, H., Hoffmann, K., and Passarge, E. (2010). Marfan syndrome with neonatal progeroid syndrome-like lipodystrophy associated with a novel frameshift mutation at the 3′ terminus of the FBN1-gene. Am. J. Med. Genet. A. *152A*, 2749–2755.

Horn, D., and Robinson, P.N. (2011). Progeroid facial features and lipodystrophy associated with a novel splice site mutation in the final intron of the FBN1 gene. Am. J. Med. Genet. A. *155A*, 721–724.

Jacquinet, A., Verloes, A., Callewaert, B., Coremans, C., Coucke, P., de Paepe, A., Kornak, U., Lebrun, F., Lombet, J., Piérard, G.E., et al. (2014). Neonatal progeroid variant of Marfan syndrome with congenital lipodystrophy results from mutations at the 3′ end of FBN1 gene. Eur. J. Med. Genet. *57*, 230–234.

Lönnqvist, L., Reinhardt, D., Sakai, L., and Peltonen, L. (1998). Evidence for furin-type activity-mediated C-terminal processing of profibrillin-1 and interference in the processing by certain mutations. Hum. Mol. Genet. *7*, 2039–2044.

Magnusson, I., Rothman, D.L., Katz, L.D., Shulman, R.G., and Shulman, G.I. (1992). Increased rate of gluconeogenesis in type II diabetes mellitus. A 13C nuclear magnetic resonance study. J. Clin. Invest. *90*, 1323–1327.

Milewicz, D.M., Grossfield, J., Cao, S.N., Kielty, C., Covitz, W., and Jewett, T. (1995). A mutation in FBN1 disrupts profibrillin processing and results in isolated skeletal features of the Marfan syndrome. J. Clin. Invest. *95*, 2373–2378.

Nickel, W. (2003). The mystery of nonclassical protein secretion. A current view on cargo proteins and potential export routes. Eur. J. Biochem. *270*, 2109–2119.

O'Neill, B., Simha, V., Kotha, V., and Garg, A. (2007). Body fat distribution and metabolic variables in patients with neonatal progeroid syndrome. Am. J. Med. Genet. A. *143A*, 1421–1430.

Pereira, L., Lee, S.Y., Gayraud, B., Andrikopoulos, K., Shapiro, S.D., Bunton, T., Biery, N.J., Dietz, H.C., Sakai, L.Y., and Ramirez, F. (1999). Pathogenetic sequence for aneurysm revealed in mice underexpressing fibrillin-1. Proc. Natl. Acad. Sci. USA *96*, 3819–3823.

Saha, P.K., Reddy, V.T., Konopleva, M., Andreeff, M., and Chan, L. (2010). The triterpenoid 2-cyano-3,12-dioxooleana-1,9-dien-28-oic-acid methyl ester has potent anti-diabetic effects in diet-induced diabetic mice and Lepr(db/db) mice. J. Biol. Chem. *285*, 40581–40592.

Takenouchi, T., Hida, M., Sakamoto, Y., Torii, C., Kosaki, R., Takahashi, T., and Kosaki, K. (2013). Severe congenital lipodystrophy and a progeroid appearance: Mutation in the penultimate exon of FBN1 causing a recognizable phenotype. Am. J. Med. Genet. A. *161A*, 3057–3062.

Trayhurn, P., Bing, C., and Wood, I.S. (2006). Adipose tissue and adipokines–energy regulation from the human perspective. J. Nutr. *136* (*Suppl 7*), 1935S–1939S.